Transactions, SMiRT-24
BEXCO, Busan, Korea - August 20-25, 2017
Division II

CREEP CRACK INITIATION AND GROWTH ASSESSMENT IN A DISSIMILAR WELD FOR NUCLEAR POWER PLANT APPLICATION

K. Abburi Venkata[1], S. Khayatzadeh[2], C.E. Truman[3]

[1] Post-Doctoral Research Associate, Department of Mechanical Engineering, University of Bristol, UK
[2] Research Fellow, Advanced Forming Research Centre, University of Strathclyde, UK
[3] Professor, Department of Mechanical Engineering, University of Bristol, UK

ABSTRACT

Creep crack initiation (CCI) and ensuing crack growth (CCG) is a potential failure mechanism in components operating at high temperatures. Reliable and correct estimation of CCI and CCG is therefore of paramount importance to ensure the safety of these components in service. The standard method of determining these parameters is to subject pre-cracked specimens to static or quasi-static loading at elevated temperatures. In the current paper, the creep crack initiation time and subsequent growth rate were studied, in a dissimilar weld used in nuclear power plants. The welded plate is made from 316LN stainless steel and P91 ferritic steel using autogenous electron beam (EB) welding. For the proposed study, a pre-cracked compact tension C(T) specimen, extracted from the welded plate, was subjected to loading at 650 °C. The load and the temperature were chosen such that they correspond to the actual service conditions. Based on the experimental investigations, the CCI time, which is the time to reach an initial crack extension of 0.2 mm and the CCG rate were identified. Also, the creep fracture mechanics parameter C^* corresponding to the crack-tip driving force under steady-state creep conditions was estimated which can be used as a material property.

INTRODUCTION

Engineering components operating at high temperatures such as steam generators, heat exchangers are susceptible to failure through creep crack growth (CCG). Usually these components are joined to other parts in the power plant using a variety of welding processes. As welding process leads to residual stresses and defect sites in the component, especially in the fusion zone and heat affected zone, it is essential to study the behaviour of a defect in such a component at elevated temperature and provide an assessment of safe life for these materials and components in service. The R5 and RCC-MR assessment procedures provide guidelines to assess whether a defect will grow to a critical size in the service life of the component for the given loading history. The design codes use linear and/or non-linear fracture parameters such as K or C^* to estimate crack initiation and growth rate at elevated temperatures [Ainsworth, 1982].

The current material under investigation is a part of feasibility study proposed for the Prototype Fast Breeder Reactor (500 MWe) which is a solid cooled fast breeder nuclear reactor presently under commission in Kalpakkam, India [Puthiyavinayagam et al., 2010]. The steam generator made of ferritic/martensitic modified 9Cr-1Mo (P91) steel is connected to the intermediate heat exchanger made of AISI 316LN stainless steel using a tri-metallic transition joint and employs a multi-pass tungsten inert gas (TIG) welding [Raj et al., 2004]. A feasibility study is proposed to explore the suitability of electron beam (EB) welding to replace the existing tri-metallic transition joint with a simple weld joint. To that end, a dissimilar metal joint is manufactured between P91 and 316LN using EB welding.

In order to study the suitability and performance of the joint, several CCI and CCG rate tests were conducted on cross-weld C(T) specimens extracted from the welded plates after the welded plates were subjected to post-weld heat treatment to relax the residual stresses. The details of the welding process,

post-weld heat treatment process, C(T) specimen extraction are explained in the next section. Based on the creep crack tests conducted on the specimens the creep fracture of this weld is studied. The results are presented and discussed in subsequent sections.

MATERIALS AND SPECIMEN DETAILS

The welded plate is a dissimilar metal joint made from ferritic/martensitic modified 9Cr-1Mo steel commercially known as P91 joined to AISI 316LN austenitic stainless steel using EB welding. The chemical composition of the base materials is shown in Table 1. The dimensions of the welded plate were 250 mm x 155 mm x 11 mm. The width of the fusion zone was ~ 1.4 mm and the heat affected zone (HAZ) on P91 side is ~ 0.8 mm. The weld pass was a full penetration pass followed by a cosmetic/smoothing pass with a penetration depth of ~ 4.5mm. The complete details of the welding process are explained elsewhere [Abburi Venkata et al., 2016]. However, the cross-sectional weld macrograph is depicted in Figure. 1. The plates were extensively characterised through residual stress measurements using neutron diffraction on strain diffractometer ENGIN-X at ISIS facility in Oxford along with residual stress predictions from numerical simulation of the welding process. Further microstructural characterisation was conducted on the plates using electron backscattering diffraction (EBSD) and hardness testing to determine the phase mixture in the weld fusion zone. The details of these studies are discussed elsewhere [Abburi Venkata et al., 2017].

In the next stage, the specimen was subjected to a post-weld stress-relief heat treatment to relax the residual stresses from the welding process and to achieve the required microstructure by reducing the hardness of the material in the weld fusion zone. The heat treatment was subjected at 760 °C for 3 h as recommended by the ASME standards for pressure vessels [ASME]. The residual stresses in the plate post to the heat treatment process were measured using contour method as well as predictions from FE model of stress relaxation. These are not discussed here and are currently under submission to another journal. The hardness of the plate across the weld from the region corresponding to the weld pass alone, was measured after post-weld heat treatment. The micro-hardness profile across the weld at mid-thickness of the specimen is shown in Figure. 2. It can be seen from Figure 2, that although post-weld heat treatment (PWHT) reduces the hardness in the weld fusion zone and P91 HAZ, the hardness is still relatively high, especially in the fusion zone. Subsequently, a cross-weld C(T) specimen was extracted from the centre of the weld using electrical discharge machining (EDM) to minimise the machining effects on the specimen residual stress state.

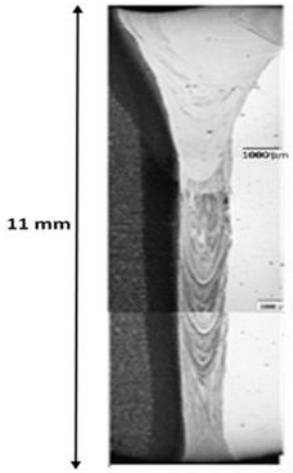

Figure 1. Weld cross-sectional macrograph

Later an EDM notch was introduced in the centre of the C(T) specimen coinciding with the weld centreline. The EDM notch was introduced along the fusion line using 0.1 mm wire for a length of 2 mm. The schematic of the C(T) specimen with the location of the EDM notch and the various regions is indicated in Figure 3. The C(T) specimen was further machined with side-grooves at an angle of 45° and 1.2 mm depth, to achieve a straight crack front. However, the machining of the side-grooves has resulted in a groove angle of 45° on the top face (with cosmetic pass) and 60° on the bottom face (weld pass) due to technical error.

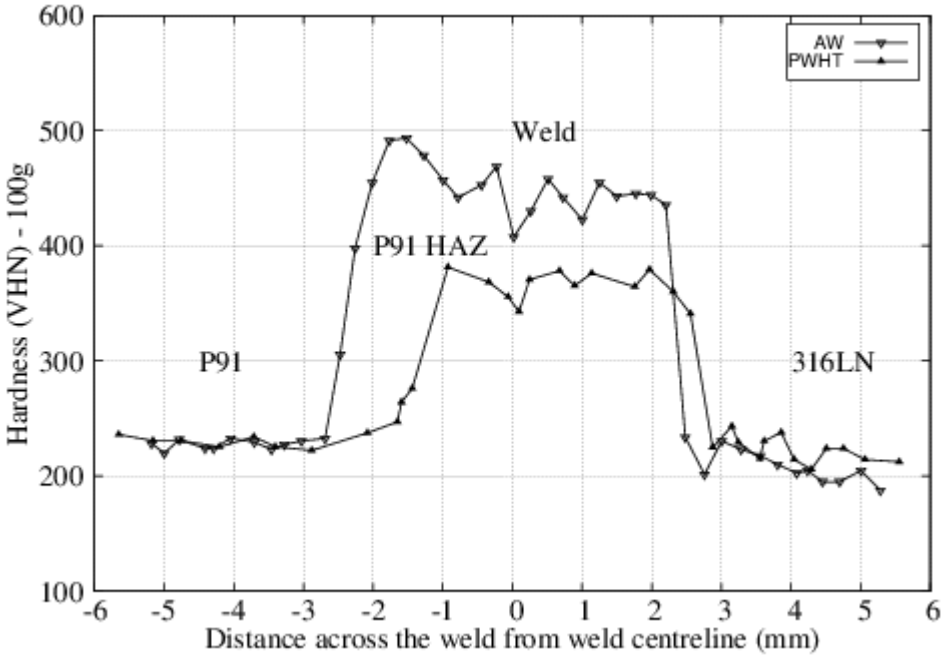

Figure 2. Hardness-map across the weld at 1.5 mm below top surface in AW and PWHT condition

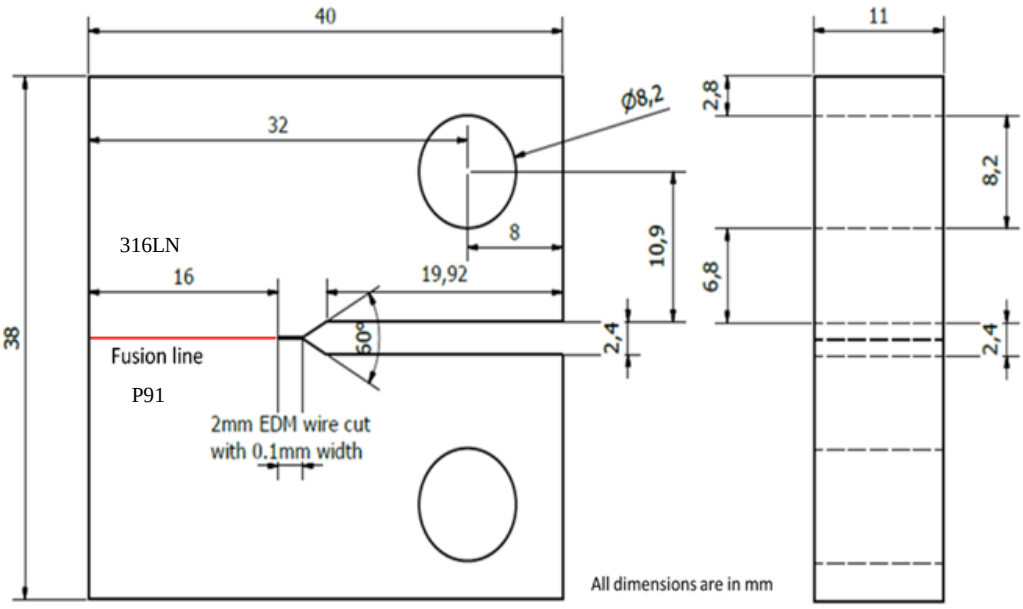

Figure 3. Schematic of the C(T) specimen with the location of the crack along fusion line

Table 1. Chemical composition of the base materials in % wt. (Balance Fe).

Steel	C	Mn	Zr	Si	P	S	Cr	Mo	Ni	Cu	Al	N	Nb	Ti	V
P91	0.11	0.39	0.005	0.27	0.017	<0.003	8.82	0.82	0.21	0.17	0.02	0.0464	0.07	0.004	0.2
316LN	0.03	1.72	-	0.39	0.025	<0.003	17.5	2.58	11.9	0.195	0.001	0.087	0.005	0.005	0.051

CREEP CRACK GROWTH EXPERIMENT

Crack initiation and growth rates at high temperatures are often assessed using fracture mechanics parameters such as stress-intensity factor (K), elastic-plastic fracture parameter (J), the reference stress (σ_R) and the creep fracture parameter (C*). The parameters K and J are generally applied for relatively short time tests where fracture is predominantly influenced by plasticity around the crack-tip [Nikbin, 2013]. Nevertheless, for longer time tests, where steady-state conditions have reached, creep fracture parameter (C*) is used to describe the stress/strain distributions ahead of the crack-tip.

In the current experiment, the reference stress method was employed to carry out the test on C(T) specimen according to the recommendations from ASTM E1457 standard [ASTM]. The reference stress was applied using limit load analysis in a structure with a flaw [Hyde (2011), Ainsworth and Lei (2009)]. The reference stress for the test specimen was calculated using Equation 1 as specified below.

$$\sigma_{ref} = \frac{P}{n_L B_n W} \tag{1}$$

where B_n and W are effective thickness with side-grooves and width of the C(T) specimen respectively. n_L is a dimensionless quantity and depends on the yield criterion and whether plane stress or plane strain condition is assumed. For a C(T) geometry, a von-Mises yield criterion with plane stress condition can be defined, based on which the value of n_L is given through Equation 2.

$$n_L = \sqrt{(1+\gamma)(1+\gamma(a/w)^2} - (1+\gamma(a/W)) \qquad 0 \le a/W \le 1 \tag{2}$$

where a is the initial crack length of the C(T) specimen, γ = 2/3. For plane strain condition, the above relation can be specified as given in Equation 3. Based on the specimen geometry and dimensions a plane stress von-Mises criterion was assumed as proposed by A.G. Miller in [Miller, 1988].

$$n_L = \gamma[\sqrt{2.702 + 4.599(\frac{a}{w})^2} - (1+1.072(\frac{a}{w}))] \qquad 0.09 \le a/W \le 1 \tag{3}$$

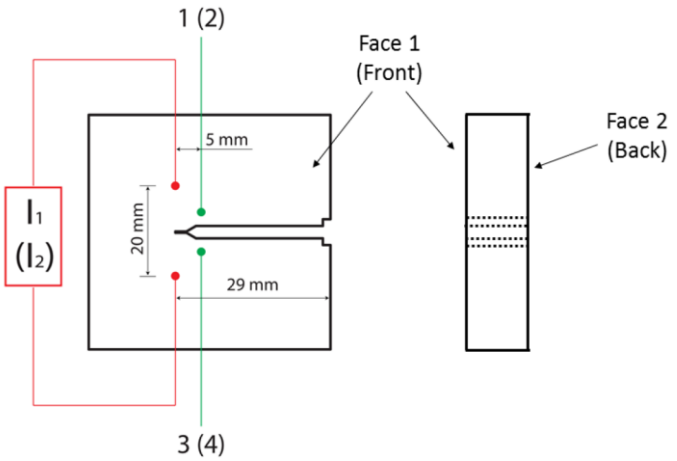

Figure 4. Schematic of the position of the Voltage and Current connections on C(T) specimen

The creep crack initiation (CCI) time and the creep crack growth (CCG) rate were measured in the C(T) specimen at 650 °C and 80 MPa of reference stress. The test is conducted using dead weight loading method. The C(T) specimen was loaded using screw loading [Khayatzadeh, 2015]. Thermocouples were attached on their surface and at the crack mouth to regulate the test temperature. In order to measure the load line displacement (LLD), linear variable differential transformer (LVDT) was attached to the specimen. Further, to measure the crack growth rate, potential drop method was employed using a direct current potential drop (DCPD) monitor. The electrical wiring attached to the specimen on front face is indicated in the schematic in Figure 4 and is repeated exactly on the back face. The initial and the final potential difference (PD) readings correspond to the initial and final crack size respectively.

EXPERIMENTAL RESULTS AND DISCUSSION

Metallography

After the test has been interrupted by continuously monitoring the PD data and LLD recorded, the specimen was broken into two halves in a tensile testing rig. One half of the specimen was used to derive the final crack length which is then used to determine the crack initiation time and growth rate. The second half was used for metallographic inspection to observe the damage ahead of the crack-tip and if there is any crack deflection into P91 HAZ resulting in a Type IV kind of failure [Shibli and Starr (2007)]. The measured average crack length is 2.8 mm and is shown in Figure 5. Also, it can be seen that the crack front is not straight and that the crack has extended further on one face than the other. This may be attributed to the difference in the side groove angle from the top face (45°) to the bottom face (60°). This change in the side-groove angle potentially alters the amount of constraint ahead of the crack-tip thereby crack-extension rate. However, this effect has to be studied further and validated with experiments to eliminate any material property/microstructure related effects.

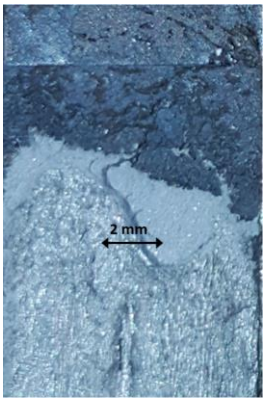

Figure 5. Measured crack front in the C(T) specimen

The region ahead of the crack-tip was examined using scanning electron microscopy (SEM) in order to investigate the potential failure mechanisms. The SEM images are displayed in Figure 6. Observing the images on left side in Figure 6(a), which is taken from the creep crack growth region, it can be inferred that the potential degradation mechanism is intergranular crack propagation with carbide precipitation at the grain boundaries. Figure 6(b) corresponds to the location at the interface of the creep crack growth and the room temperature ductile fracture associated with opening of the crack faces under tension. Here the ductile pores from the room temperature fracture can be clearly seen. Nevertheless, the specimen indicates heavy oxidation of the fracture surfaces rendering it hard to determine the failure mechanism accurately. A further detailed microscopy through electron back-scattering diffraction

(EBSD) shall be undertaken on the fracture surfaces to provide more information on the underlying degradation mechanisms.

A reconstruction of the crack face using a surface profiler instrument is shown in Figure 7. The purpose of the reconstruction was to verify the crack propagation path was straight, without deflection into P91 HAZ (indicative of Type IV failure) [Shibli and Starr (2007)]. However, observing the profile of the crack it can be commented that the crack propagation was straight and confined to the weld fusion line without any deflection into the Type IV region.

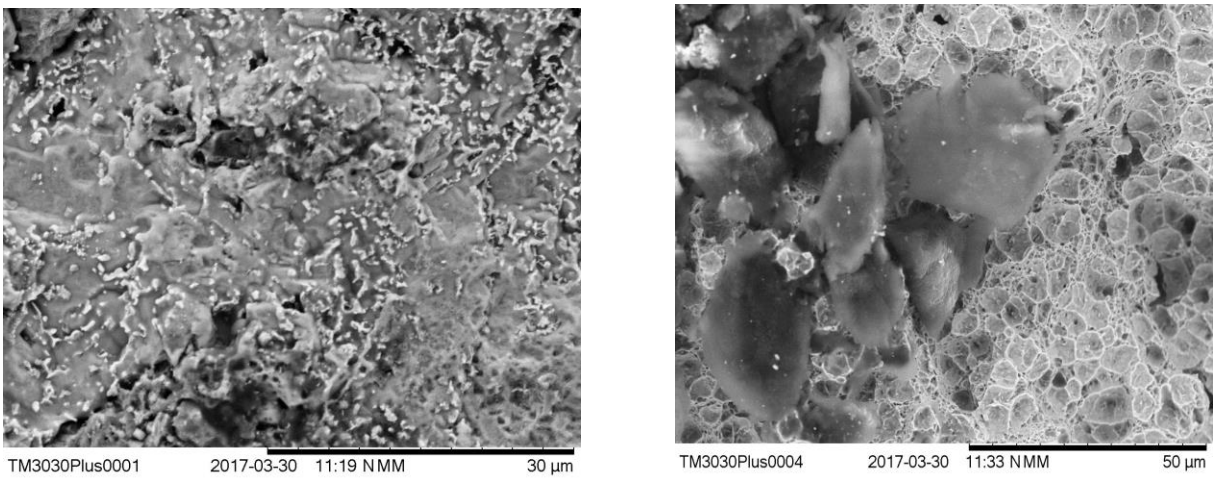

(a) (b)

Figure 6. SEM images of the fracture surface (a) in the creep crack growth region (b) interface of creep crack growth and ductile fracture of the C(T) specimen at room temperature

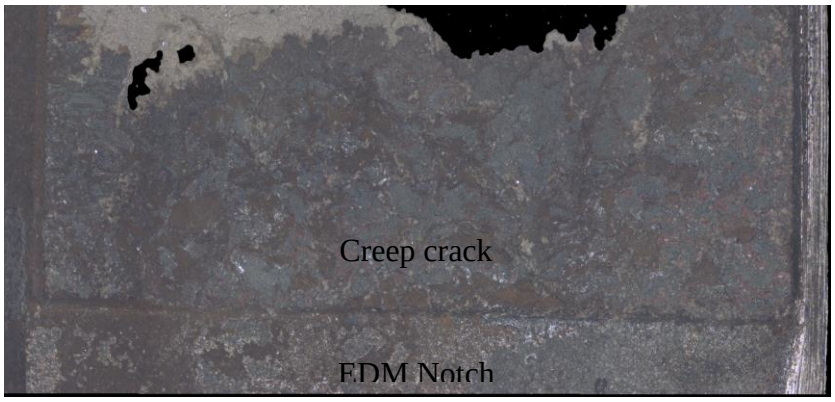

Figure 7. Reconstruction of the crack front on surface profiling instrument

Creep crack initiation time and growth rate

Based on the electrical PD, force, LLD measured during the experiment, the crack initiation time and crack growth rate were determined. The load line displacement vs time is shown in Figure 8. The creep crack growth rate curve is depicted in Figure 9. The initial and final PD readings correspond to the initial and final crack sizes, respectively during the test. Therefore, at intermediate points, instantaneous crack size can be determined by linear interpolation of the PD data based on the initial and final crack length measured on the fracture surface.

The crack length at any instant can be specified using the relation

$$a = \left[(a_f - a_0) \frac{(V - V_0)}{(V_f - V_0)} \right] + a_0 \tag{4}$$

where V_0 and V_f are the initial and final PD readings, V is the instantaneous potential difference corresponding to the crack size *a*. a_f and a_0 are the final and initial crack size. The crack initiation time can be defined as the time required for an initial crack extension size of 0.2 mm. Based on this definition, the crack initiation time can be determined as ~ 207 h for this material, for the given temperature and loading conditions.

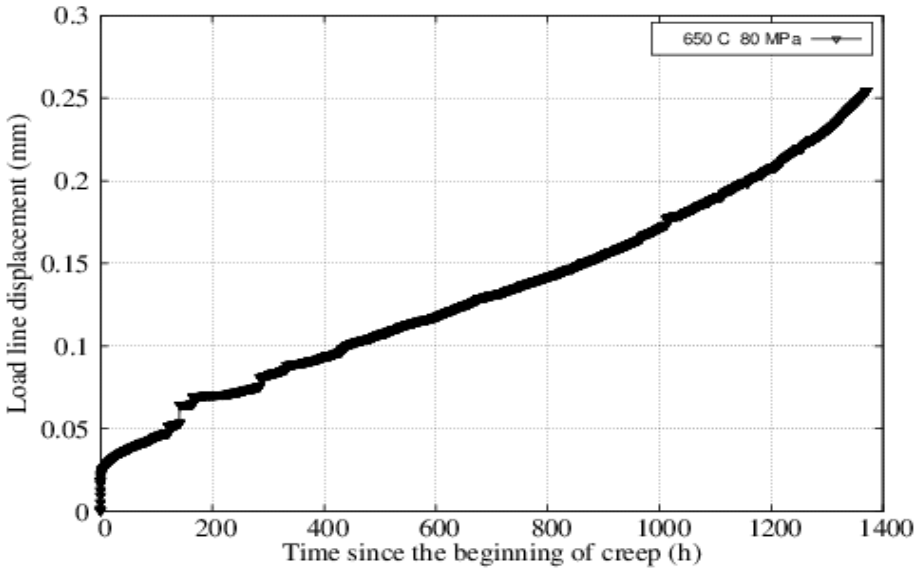

Figure 8. Graph depicting the load line displacement (LLD) vs creep time

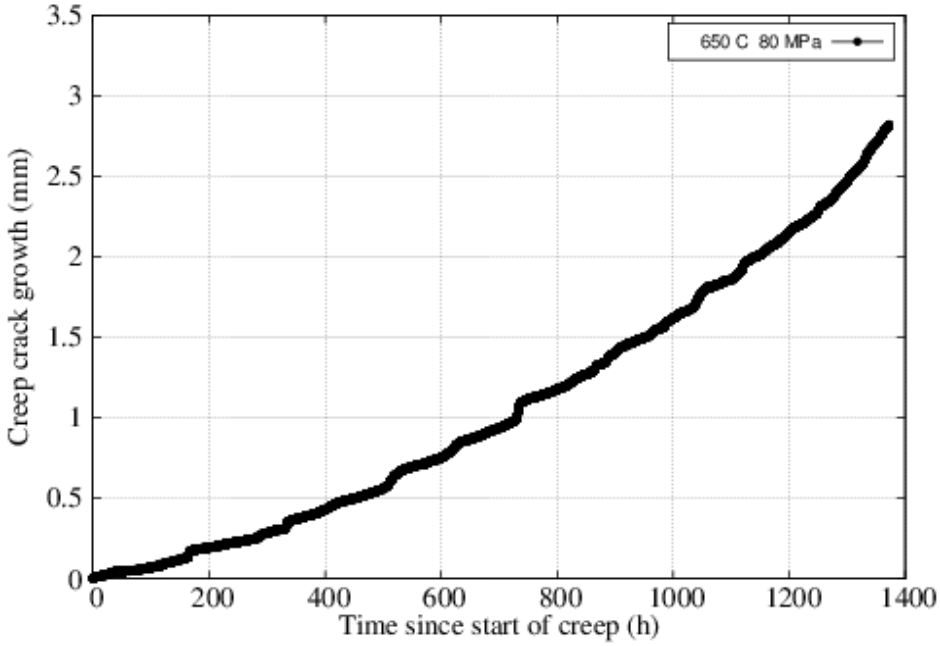

Figure 9. Creep crack growth vs time for dissimilar metal weld at 80 MPa reference stress

Comparison of crack initiation time with a similar weld

The creep crack initiation time as well as the crack growth measured for the current specimen is compared with that of a similar weld made from P91 material. The comparison of the crack growth rate curves is shown in Figure 10. The comparable dimensions for the three specimens are displayed in Table 2.

The dissimilar weld and similar weld specimens are cross-weld C(T) specimens with cracks located in the centre of the fusion zone. From Table 2, it can be seen that the crack dimensions are same for all the three specimens. However, the thickness of the specimen is different for the dissimilar welded specimen and therefore the load applied. Looking at the graph, it is observed that the crack initiation time for the dissimilar weld is longer than that of the similar P91-P91 cross-weld specimen. Nevertheless, this has to be further validated for specimen with exact geometry.

Table 2. Specimen geometry and creep crack characterisation for various materials [Khayatzadeh, (2015)]

Material	Reference Stress (Plane stress condition) (MPa)	Width of the specimen (W) (mm)	Initial crack length (a) (mm)	Thickness of the specimen (B) (mm)	Net thickness of the specimen (Bn) (mm)	Load applied (F) (kN)	Crack initiation time for 0.2 mm crack growth (h)
Parent P91	80	32	16	8.24	5.88	1.33	549
CW P91-P91	80	32	16	8.24	6.11	1.37	96
DMW P91-316L	80	32	16	10.95	9.15	2.1	207

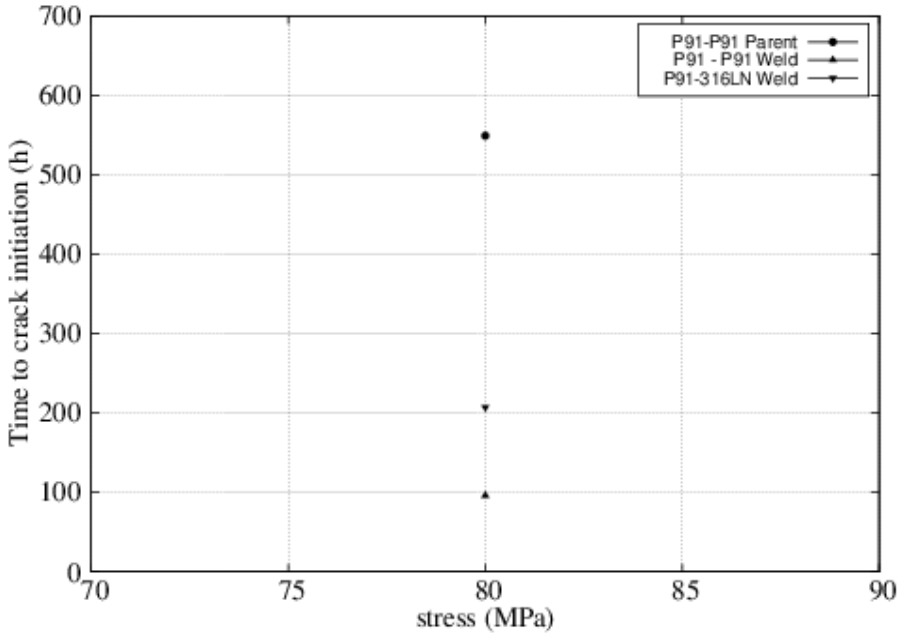

Figure 10. Comparison of crack initiation (0.2 mm crack growth) time between P91 parent, weld and dissimilar weld C(T) specimens

C* parameter determination

Further to the crack growth rate, the fracture mechanics parameter *C** has been applied in this paper to explore the rate of crack growth:

$$\dot{a} = DC^{*\varphi} \tag{5}$$

where D and φ are temperature and stress dependent material constants. In the present research, *C** has been computed experimentally, as suggested by the ASTM E1457 standard [8], using the rate of load line displacement for compact tension (C(T)) specimen:

$$C^{*} = \frac{n}{n+1}\frac{P\dot{\Delta}}{B_n(W-a)}\eta \tag{6}$$

where $\dot{\Delta}$ is the rate of creep load line displacement, P is load, n is secondary creep exponent, a is initial crack length, W is width of C(T) specimen, and B_n is the net section of C(T) specimen with side grooves, η is a constant based on the specimen geometry and weld mismatch factors. The creep exponent is calculated as 9.18 based on cross-weld creep rupture tests conducted at 650 °C at a stress range of 80 MPa to 120 MPa. Based on the assumption that the weld is an overmatch to the parent, the value of η is taken as 2.0 as per ASTM E1457standard [8]. The *C** parameter was calculated for the current material under consideration based on the load line displacement rate. The variation of crack growth rate with *C** is depicted in Figure 11. This parameter can be correlated against crack growth rate based on multiple tests and can be used as a material property to evaluate the creep crack growth rate under steady-state. In this paper, the results from a single test are presented. Subsequently more creep crack growth tests shall be conducted to evaluate *C** parameter as a material property.

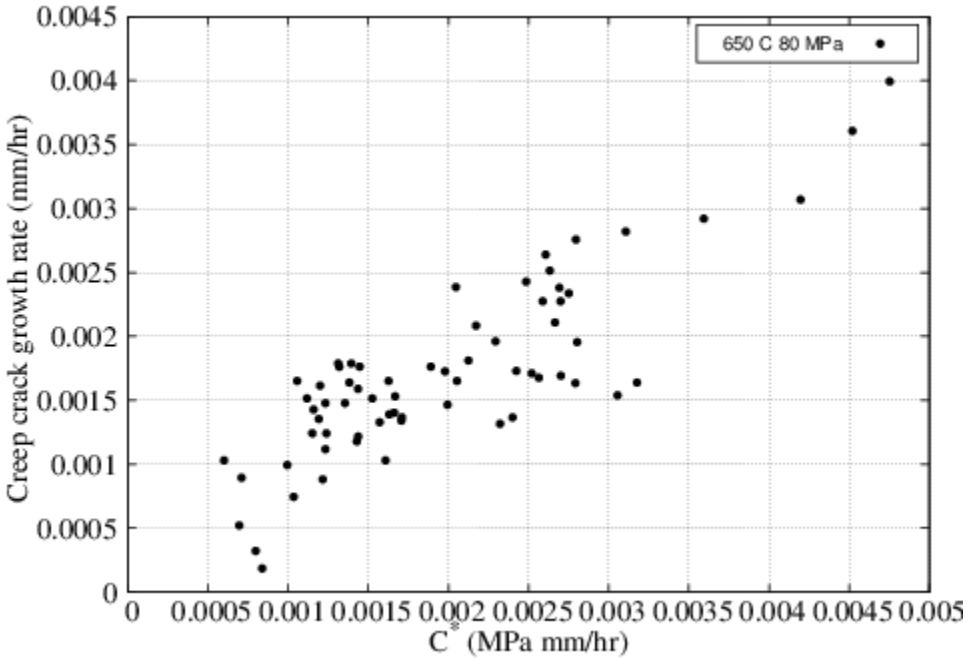

Figure 11. Creep crack growth rate vs C* for the dissimilar weld at 80 MPa reference stress

CONCLUSIONS

Based on the creep crack growth tests conducted on this material for crack located in the weld fusion zone, the following conclusions could be made:

1. The total crack length of ~ 2.8 mm was measured after a test duration of ~1400 h.
2. The crack initiation occurred at ~ 200 h after the test has been started.
3. The crack front was not straight. This has been attributed to the different constraint levels arising from the differences in the side-groove angle on the top and bottom face of the C(T) specimen. However, this needs to be verified by further tests to study the material composition variation effects from weld and cosmetic passes.
4. The creep crack initiation comparison of the dissimilar weld under investigation with that of similar weld made from P91 indicates a slower crack initiation time for the dissimilar weld.

REFERENCES

Abburi Venkata, K. Truman, C.E. Smith, D.J. Bhaduri, A.K. (2016) "Characterising electron beam welded dissimilar metal joints to study residual stress relaxation from specimen extraction" *International Journal of Pressure Vessels and Piping*, 139 – 140, 237 – 249.

Abburi Venkata, K. Coules, H.E. Truman, C.E. Warren, A.D. (2017) "Applying electron backscattering diffraction to macroscopic residual stress characterisation in a dissimilar weld" *Journal of Materials Processing Technology*, 241, 54 – 63.

Ainsworth, R.A. (1982). "Some observations on creep crack growth" *International Journal of Fracture*, 20: 147 – 159.

Ainsworth, R.A. Lei, Y. (2009). "Creep crack growth assessment methods" *Anales de Mecánica de la Fractura* 26(1).

ASME Boiler and Pressure Vessel Code, Sections I, II and IX and B31.1.

ASTM E 1457-01. (2001) "Standard Test Method for Measurement of Creep Crack Growth Rates in Metals", ASTM Standards.03.01.

Hyde, T.H. (2011). "The Use of the Reference Stress Concept in Creep Crack Growth Studies" *Journal of the Mechanical Behaviour of Materials*, 2.1-2: 37-56. Retrieved 1 May. 2017, from doi:10.1515/JMBM.1989.2.1-2.37

Khayatzadeh, S. (2015). "*Creep deformation and crack incubation of martensitic steels under different boundary conditions*", PhD Thesis, University of Bristol.

Miller, A.G. (1988). "Review of limit loads of structures containing defects" *International Journal of Pressure Vessels and Piping*, 32: 197 – 327.

Nikbin, K. (2013) "Creep/Fatigue Crack Growth Testing, Modelling and Component Life Assessment of Welds" *Procedia Engineering*, 55, 380 – 393.

Puthiyavinayagam, P. Raghupathy, S. Balasubramaniyan, A. Selvaraj, P. Mohanakrishnan, P. Chetal, S.C., Chellapandi, P. Raj, B. (2010). "Current status of fast reactors and future plans in India", *Energy Procedia*, 7: 64 – 73.

Raj, B. Bhoje, S.B. Mannan, S.L. Chetal, S.C. (2004). "Selection of materials for prototype fast breeder reactor", *Transactions of Indian Institute of Metals*, 56(2): 155 – 178.

Shibli, A. Starr, F. (2007). "Some aspects of plant and research experience in the use of new high strength martensitic steel P91" *International Journal of Pressure Vessels and Piping*, 84, 114 – 122.